ELSEVIER

Dynamics of Atmospheres and Oceans
37 (2003) 1–24

dynamics of atmospheres and oceans

www.elsevier.com/locate/dynatmoce

Nonmodal and unstable normal mode baroclinic growth as a function of horizontal scale

Daniel Hodyss*, Richard Grotjahn

Atmospheric Science Program, Department of Land, Air and Water Resources, University of California, One Shields Avenue, Davis, CA 95616, USA

Received 19 July 2002; received in revised form 18 September 2002; accepted 22 October 2002

Abstract

Linear, quasi-geostrophic, Cartesian, spectral models based on Grotjahn (1980) are solved as initial-value problems. The basic-state wind flow includes realistic vertical shear in the form of an upper-level jet but no horizontal shear. Two archetype initial vertical structures are selected. One structure, labeled "connected", develops strong nonmodal growth (NG). The other structure, labeled "separated", is intended to approximate better conditions prior to observed cyclogenesis. NG is deduced from growth rates of common growth measures: amplitude, total energy, potential enstrophy, and their components. Significant NG may occur, usually early on, before a solution asymptotes to the most unstable normal mode. This study focuses on how the relative amounts of NG and unstable normal mode growth vary for different scales in both horizontal dimensions.

The peak NG in most growth measures is greatest for wavelengths much smaller than the most unstable normal mode wavelength. The peak NG occurs earlier as wavelength decreases consistent with relative phase speed and distance arguments applied to constituent eigenmodes coming into favorable superposition. The peak NG is much less at all wavelengths for a separated trough than a connected initial condition (IC), except for the boundary contribution to potential enstrophy. Also, the connected IC has peak NG at shorter wavelengths than the separated IC. The peak NG occurs at a shorter wavelength for amplitude than for total energy. The connected and separated ICs are shown with the horizontal structure of a square wave and for a wave having initially localized structure along the meridional axis but allowed to evolve in that dimension. The main differences are initially localized waves develop larger meridional scale and commensurately larger growth rates. When the meridional structure is allowed to evolve, transient horizontal tilts appear leading most commonly to zonal mean convergence of eddy momentum. Phase speed differences between the main eigenmodes comprising the total solution primarily explain this result.

Keywords: Dynamical theory; Baroclinic instability; Nonmodal growth; Quasi-geostrophic model; Energy growth; Enstrophy growth; Linear instability

* Corresponding author. Fax: +1-530-752-1552.
E-mail address: dhhodyss@ucdavis.edu (D. Hodyss).

0377-0265/02/$ – see front matter © 2002 Elsevier Science B.V. All rights reserved.
PII: S0377-0265(02)00064-7

1. Introduction

The primary aim of this article is to identify how the relative importance of nonmodal growth (NG) and unstable normal mode growth (UNMG) varies for different horizontal scales of a simulated extratropical cyclone. Two sets of simulations are run using linear, quasi-geostrophic (QG) models. In one set the meridional (l) and zonal (k) wavenumbers are set equal, creating waves that are labeled "square" waves because of their appearance when plotted: the "zero" contours look like squares. (These are not plane waves.) Setting $k = l$ recognizes that most observed frontal cyclones have similar zonal and meridional scales in the geopotential height fields (e.g. Grotjahn and Castello, 2000). In the other set of simulations k remains a single wavenumber, but the meridional structure is free to evolve over time from an initial Gaussian profile. In each set of simulations two archetype initial conditions (ICs) are considered: one that favors NG (vertically connected troughs and ridges; hereafter labeled "connected") and one that approximates observed conditions prior to cyclogenesis (separate upper and lower troughs and ridges, neither having tilt; hereafter labeled "separated"). The relative presence of NG or UNMG is identified using time series of the growth rates of amplitude norm ($L2$), and mass-integrated total energy (E) and potential enstrophy (H). Those H and E growth measures are further subdivided into their components so as to understand better the source of the NG.

Prior work on NG has emphasized the dynamics of the process (e.g. Farrell, 1982, 1984); optimal structures (Farrell, 1989); how NG varies with IC (e.g. Grotjahn et al., 1995; Grotjahn and Tribbia, 1995); the structure at peak growth (e.g. O'Brien, 1992); and other factors. This prior work often treats the meridional structure in a simple way (for example, by assuming no meridional variation).

Preliminary work to understand the effect of horizontal scale and structure on NG has generally been carried out with simple models. Davies and Bishop (1994) address how NG varies with horizontal scale in the context of Eady edge waves having zero interior quasi-geostrophic potential vorticity (QGPV). They do however provide a brief description of the effect of including interior delta function QGPV anomalies but in a context that excludes growing normal modes. They find for Eady edge waves having zero interior QGPV that the most rapidly growing horizontal scale depends on the growth measure they choose to examine for NG. The maximum growth rate takes place at large (small) wavelengths for the boundary temperature (pressure) growth measure. Hakim (2000b) considers NG in the presence of growing normal modes for basic-states with uniform QGPV. He defines his IC in terms of QGPV as an isolated upper-level anomaly. Hakim includes two different sized ICs in a table showing growth over 48 h. Hakim's table indicates that the shorter IC has larger growth of energy and QGPV but less growth of amplitude and surface pressure minimum. He felt that a larger upper-level disturbance could induce stronger surface development since the larger disturbance had a much greater projection onto the most unstable normal mode. Hakim uses zonally and meridionally localized ICs. Because our work is focused on how scale affects the growth mechanisms, we isolate that scale by allowing only a single zonal wavenumber for each solution. An in-depth discussion of the relationship between our work and Hakim (2000b) can be found in Section 2.2. Badger and Hoskins (2001) examine NG at varying horizontal scales in an Eady-type model with ICs

consisting of zonally isolated perturbations in the pressure field. The growth measure that they choose is the domain averaged kinetic energy. They find that the shortest scale waves have the greatest NG, but that the length of time that NG occurs is shortest for the shortest waves.

The study described here extends this previous work in two specific ways: (1) by using a more "realistic" basic-state with fewer assumptions than the Eady (1949) model and; (2) by comparing and contrasting the various growth measures that are typically used in the literature and their components. The model used here includes a "realistic" vertical profile of basic-state QGPV as well as an interior distribution of perturbation QGPV. Furthermore, while some studies choose to define their IC based on observed upper-level potential vorticity precursors (e.g. Hakim, 2000b) we define the IC here based on observed precursors in the pressure field (Grotjahn, 1996). Also, the widely differing growth measures used throughout the literature make it difficult to compare growth rates and consequently the amount of NG between studies. Subsequently, quantifying whether NG occurs in a particular model and IC based on one growth measure can be misleading. As shown in Hodyss and Grotjahn (2001) each of the three most common growth measures (H, E, $L2$) emphasizes a different part of the growth and structural change that occurs during cyclogenesis. This article examines NG at various horizontal scales, focusing on how H, E, $L2$ and the components of H and E evolve over time.

Section 2 describes the model and the diagnostic calculations used to evaluate the growth and evolution of cyclones at various horizontal scales. Section 3 shows results for "square waves" with a single zonal and meridional wavenumber. Section 4 shows results for *initially* square waves that have a single zonal wavenumber and a Gaussian meridional structure. Section 5 closes with a discussion of the conclusions.

2. Model and diagnostics

2.1. Model formulation

The model equations consist of nondimensional, linearized conservation of quasi-geostrophic potential vorticity (QGPV) in the interior of the domain:

$$\left[\frac{\partial}{\partial t}+U\frac{\partial}{\partial x}\right]\left(\nabla^2\varphi+\frac{1}{\rho}\frac{\partial}{\partial z}\left(\rho\varepsilon\frac{\partial\varphi}{\partial z}\right)\right)+\frac{\partial Q}{\partial y}\frac{\partial\varphi}{\partial x}=0 \tag{1}$$

where φ is the perturbation stream function and $U=U(z)$ is the prescribed zonal wind.

$\partial Q/\partial y=\beta-(1/\rho)(\partial/\partial z)(\rho\varepsilon(\partial U/\partial z))$ is the meridional gradient of the prescribed or "basic-state" potential vorticity Q; β the nondimensional meridional derivative of f, the Coriolis parameter, appropriate for midlatitude scaling, $\rho=\rho(z)$ the basic-state density and $\varepsilon=(f_0D/NL)^2$, where N is the Brunt Väisälä frequency, L the horizontal length scale, D the vertical length scale, and so ε is the squared ratio of the Rossby radius of deformation over the assumed length scale. All equations presented here have been made nondimensional using typical scaling magnitudes for horizontal length ($L=1000$ km), vertical depth ($D=10$ km), speed ($V=10\,\mathrm{m\,s^{-1}}$), and the advective time scale ($L/V=10^5$ s).

Assuming rigid horizontal boundaries along the top and bottom of the channel, the boundary conditions in z are

$$\left[\frac{\partial}{\partial t} + U\frac{\partial}{\partial x}\right]\left(\frac{\partial \varphi}{\partial z}\right) - \frac{\partial U}{\partial z}\frac{\partial \varphi}{\partial x} = 0, \quad \text{at } z = 0,\ z^{\text{top}}. \tag{2}$$

The rigid horizontal boundary (2) can be interpreted as coupled to (1); hence, perturbation QGPV (Bretherton, 1966; Lindzen and Tung, 1978) will consist of three terms:

$$q = \nabla^2\varphi + \frac{1}{\rho}\frac{\partial}{\partial z}\left(\rho\varepsilon\frac{\partial \varphi}{\partial z}\right) + \varepsilon\left(\frac{\partial \varphi}{\partial z}\delta(z) - \frac{\partial \varphi}{\partial z}\delta(z - z^{\text{top}})\right) \tag{3}$$

where $\delta(z)$ is the dirac delta function. The first term in (3) is the relative vorticity (RV), the second is the "thermal" vorticity (TV), and the last is the contribution from boundary potential temperature (BPV).

The above equations will be solved for two different types of basic-states. The Eady (1949) model is recovered if $\partial Q/\partial y = 0$, $U = z$, $\varepsilon = 1$, $z^{\text{top}} = 1$, and $\rho =$ constant. The model in Grotjahn (1980; hereafter the "G" model) uses realistic vertical profiles of these quantities. The basic-state in the G model has maximum U at "tropopause level" ($z = 1.0$; based on static stability and density profiles modeled after the US Standard Atmosphere). Q in the G model is largest at 8 km, with surface values one fifth as large. Further details can be found in Grotjahn (1980) and Hodyss and Grotjahn (2001).

These equations are solved numerically using a pseudo-spectral method with the 3rd order Adams–Bashforth scheme for the time integration. The time increment is 0.005. The domain is a channel model with boundary conditions in x being periodicity and vanishing normal velocity in y. It is solved spectrally in the horizontal with second-order finite differences in the vertical. The horizontal resolution consists of one Fourier mode in x with one in y for the "square wave" simulations and 32 in y for the meridionally free simulations. The number of levels in the vertical is 31 for both sets of simulations.

2.2. Initial conditions

The archetype ICs are defined in the pressure field and are shown in Fig. 1. The functional form of the "connected" IC is

$$\varphi_{\text{c}} = \cos\left(kx + \frac{3\pi}{2}z\right)\cos(ly), \quad \text{for } z \le 1.0 \tag{4a}$$

$$\varphi_{\text{c}} = \cos\left(kx + \frac{3\pi}{2}\right)\cos(ly)\,\mathrm{e}^{-2(z-1)}, \quad \text{for } z > 1.0 \tag{4b}$$

where k, l are the zonal and meridional wavenumbers, respectively. The functional form for the "separated" IC is

$$\varphi_{\text{s}} = [\tanh[5(z - 0.3)]\cos(kx) + (1 + \tanh[5(z - 0.6)])(1 - \tanh[5(z - 1.2)])\cos(kx + \pi)]\cos(ly). \tag{4c}$$

The "connected" case has uniform amplitude with height in the troposphere and amplitude decaying with height in the stratosphere. A similar IC is examined in Grotjahn et al. (1995)

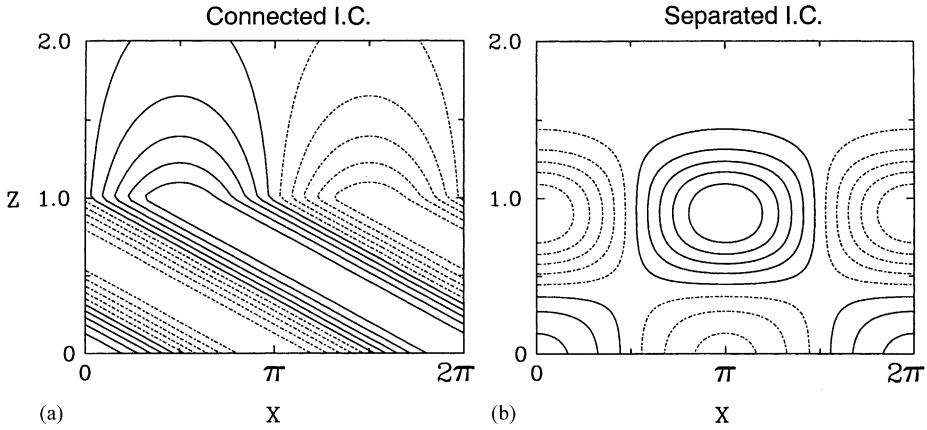

Fig. 1. Archetype initial conditions (a) connected and (b) separated shown in a zonal cross section. The former represents widely studied initial conditions that have strong nonmodal growth (NG). The latter represents initial conditions roughly similar to troughs observed prior to cyclogenesis.

for various amounts of initial upstream tilt. When calculations are made using different initial tilts, Grotjahn et al. (1995) find a relatively similar peak value of growth rate when the initial upstream tilt is at least 90° (90° refers to the phase shift upstream from the surface to the tropopause level). The amount of tilt at peak growth rate depends on the growth measure. The tilt is often larger when $L2$ growth is maximized than for E. The tilt at peak growth is roughly 90°. The peak growth rate occurs at later times for initial tilts larger than 90°. Accordingly, in this study we elect to consider just one amount of initial upstream tilt as representative of behavior for a broader class of ICs having constant amplitude with height. As discussed in Grotjahn et al. (1995) and Hodyss and Grotjahn (2001) this IC contains a significant amount of NG: peak growth rates can be more than twice the asymptotic value. This type of IC has been the archetype for developing the NG concept (Farrell, 1982, 1984) precisely because NG is so strong for this IC. The connected IC provides a benchmark against which the separated IC results may be related to earlier works using ICs similar to the connected IC. A benchmark is needed because one usually cannot directly compare growth rates between different articles in the literature because the models used will have important differences. Common differences include: the basic-state wind shear and static stability profiles, the model geometry (Cartesian or spherical), and the level of approximation (compressible or not, variable Coriolis or not, quasi-geostrophic or "primitive" equation, etc.).

The second IC is labeled the "separated" IC and is based upon observational work reported by Grotjahn (1996). Twenty-seven rapidly developing extratropical cyclones are tracked before and during cyclogenesis near the East Coast of Asia. These cyclones develop when a deep upper trough moves sufficiently close to a shallow surface-trapped trough. Takayabu (1991) also observed that development commences when a deep upper trough approaches a shallow surface trough. Takayabu referred to this as "coupling" development; a similar process appears to be commonly described in the literature as "type B" cyclogenesis (Petterssen and Smebye, 1971).

Hakim (2000b) uses analytic functions to approximate potential vorticity structures found in the atmosphere. He bases his IC on Hakim (2000a). Hakim (2000a) considers several levels but his primary focus is on the 500 h Pa level where an automated scheme tracks the relative vorticity of numerous vortices at various stages of development. His approach appears to have only identified the deep, upper-level QGPV structure that precedes development and not the QGPV associated with a shallow, surface pressure feature. We feel the shallow surface trough is an important part of an IC that is intended to simulate cyclogenesis and motivates our use of the "separated" IC.

As with the connected case, the separated IC is intended to be representative of a broader class of ICs with varying degrees of phase shift between upper and lower features. A key property is that the upper and lower troughs are not connected and each has no upstream tilt. Grotjahn and Tribbia (1995) examine a similar separated IC and find that it develops much less NG than does the connected IC. However, their separated IC has larger phase shift between upper and lower features and they only consider the most unstable normal mode wavelength. This report finds a similar result as Grotjahn and Tribbia (1995) for the most unstable wavelength despite the difference in initial phase shift. So, the results shown here are little sensitive to the initial phase shift between the upper and lower features. As with the connected IC, the primary difference is to affect the time of occurrence of the peak growth rate. Other simulations (not shown) by Grotjahn and Tribbia find that these results are not sensitive to changes of the relative upper and lower amplitudes; thus we feel justified in drawing broad conclusions from this archetype IC.

2.3. Growth measures

Several growth measures are tracked over time in this study. The integrated mass weighted total energy, E is defined as:

$$E = \frac{1}{2}\int_v \rho(\varphi_x^2 + \varphi_y^2 + \varepsilon\varphi_z^2)\,\mathrm{d}V. \tag{5}$$

For later reference, the mass weighted integral of the two components of (5) will be referred to as the kinetic energy (KE) and the available potential energy (APE) in this QG system. Potential enstrophy, H is defined as:

$$H = \frac{1}{2}\int_v \rho q^2\,\mathrm{d}V \tag{6}$$

where q is the perturbation QGPV in the numerical model formulation of (3). The mass weighted integral of each of the three components of q (3) will be tracked over time.

Amplitude growth is revealed using this norm:

$$L2 = \left(\int_v \rho\varphi^2\,\mathrm{d}V\right)^{1/2}. \tag{7}$$

See Hodyss and Grotjahn (2001) for a complete description of these growth measures. The exponential growth rates of E, $L2$, and H are the primary diagnostics used in this study. The growth rates for E and H asymptote to twice the growth rate of the most unstable normal mode.

NG is difficult to assess quantitatively since it can be present even when the growth rate is below the unstable normal mode value. If the unstable normal mode is but a small fraction of the total solution then its effect on the total growth rate may be very small allowing small to moderate NG to dominate the total growth rate. In this case the total growth rate could be below the most unstable normal mode value but still be dominated by nonmodal processes. Accordingly, one can only make a somewhat qualitative judgment based mainly upon the peak growth rate (particularly when it exceeds the most unstable normal mode value). Yet, qualitative aspects seem appropriate to emphasize here given the approximations in the models and the use of ICs as archetypes. Also, the importance of NG is assessed in relative terms by comparing results for an archetype structure found prior to observed cyclogenesis against an IC with significant NG.

The ratio of instantaneous over asymptotic growth rate at a given zonal wavenumber defines a parameter Γ. Parameter Γ facilitates comparison of the NG magnitude at different scales and between different parameters whereas the actual growth rate (plotted here) helps identify how the NG alters the growth rates seen at different time and space scales. Parameter Γ is not singular since the asymptotic growth rate is not zero for any wavenumber studied here.

3. "Square wave" results

3.1. Introductory comments

A solution that looks like a "checkerboard" pattern of highs and lows is obtained by assuming the stream function takes the form

$$\varphi(x, y, z, t) = \Phi(z, t) \sin(ly)\, \mathrm{e}^{\mathrm{i}kx} + * \tag{8}$$

where k, l are the zonal and meridional wavenumbers, respectively and * represents the complex conjugate of the preceding term. It is further assumed that $k = l$ so that the zero-valued contour line forms a square leading to the terminology "square waves".

Square waves are justified on three bases. First, square waves are sometimes used as an improvement upon plane wave solutions while still simplifying or speeding up a calculation. Second, for a feature localized along the meridional axis, having a circular circulation, the dominant member of a Fourier decomposition is that member used in the square wave. Finally, we find similar results for square waves and waves localized along the meridional axis.

One may insert (8) into the linearized QGPV Eq. (1) and obtain

$$\left[\frac{\partial}{\partial t} + \mathrm{i}kU\right]\left(\frac{1}{\rho}\frac{\partial}{\partial z}\left(\rho\varepsilon\frac{\partial \Phi}{\partial z}\right) - \alpha^2\Phi\right) + \mathrm{i}k\frac{\partial Q}{\partial y}\Phi = 0 \tag{9}$$

where α is the absolute wavenumber: $\alpha^2 = k^2 + l^2 = 2k^2$.

It is obvious that the terms in (9) scale differently with wavenumber. Accordingly, in the G model, or similar variations such as those in Green (1960), the growing normal mode solutions become more bottom-trapped as absolute wavenumber (α) increases from the scale of the most unstable mode. This well-known result strongly influences the projection

onto the eigenmodes that are present in the ICs emphasized here. For short waves, unstable normal modes must be significantly augmented by neutral continuum modes in order for the IC to have significant amplitude in the upper troposphere. In contrast, near the most unstable wavelength, unstable normal modes have relatively comparable amplitude at upper and lower troposphere and thus form a greater fraction of the IC.

As described elsewhere (e.g. Grotjahn et al., 1995, Hodyss and Grotjahn, 2001), a simple conceptual model for NG is the increasingly favorable superposition of constituent eigenmodes. The eigenmodes of the G model are not orthogonal in the growth measures mentioned above. Therefore, the superposition and differing phase speeds of the eigenmodes will induce changes with time in these growth measures. To single out just one factor, the greater the phase speed difference, the faster the transition is to a favorable alignment of two modes, and thus the greater the NG. The speed with which the eigenmodes adjust their relative phase in a favorable manner is dependent upon the relative phase speeds of the primary constituents (as well as the initial phase shifts). For example, as wavenumber increases beyond the most unstable normal mode, the time needed for a given phase speed difference between two constituent eigenmodes to shift those eigenmodes one half wavelength (say) into phase will decrease simply because the wavelength is smaller (making NG greater, all else being equal). As k increases this effect is magnified for general ICs because the unstable normal mode becomes more bottom-trapped and therefore must be augmented by more and more neutral continuum modes, which have a relatively wide range of phase speeds. So, one might anticipate more NG to occur for shorter waves than for longer waves, if only phase speed (not structure) is the issue. Of course, the precise amount of NG is not easy to deduce since it depends upon other factors that vary with wavenumber. Such other factors include the normal mode growth rate spectrum and variations in the amount of overlap between the eigenmodes. So, one can reasonably expect NG to vary with the scale of the mode, but the details of the variation are most easily deduced by direct calculation.

3.2. Time series of growth rates

Fig. 2 displays time series of the growth rates for H, E and the $L2$ norm for the G model. Time series for connected and separated ICs are shown. As expected, the solution asymptotes over time to the growing normal mode. Table 1 summarizes some key properties of the solutions for the connected and separated trough ICs in the G and Eady forms of the model. The principal results seen in *both* models and *both* ICs are these.

- The time at which the peak growth rate occurs decreases as the wavelength decreases for all growth measures.
- The peak NG occurs for wavelengths notably shorter than the most unstable normal mode for all growth measures.
- In general, the peak growth rate occurs for shorter wavelengths in the amplitude ($L2$) norm than in the total energy growth measure (E).

As stated, similar results appear in Eady model runs (not shown). The primary difference occurs where growing normal modes do not exist at wavenumbers above $\alpha = 2.4$ in the Eady model. Those short wave Eady solutions show interference effects as discussed by Lindzen

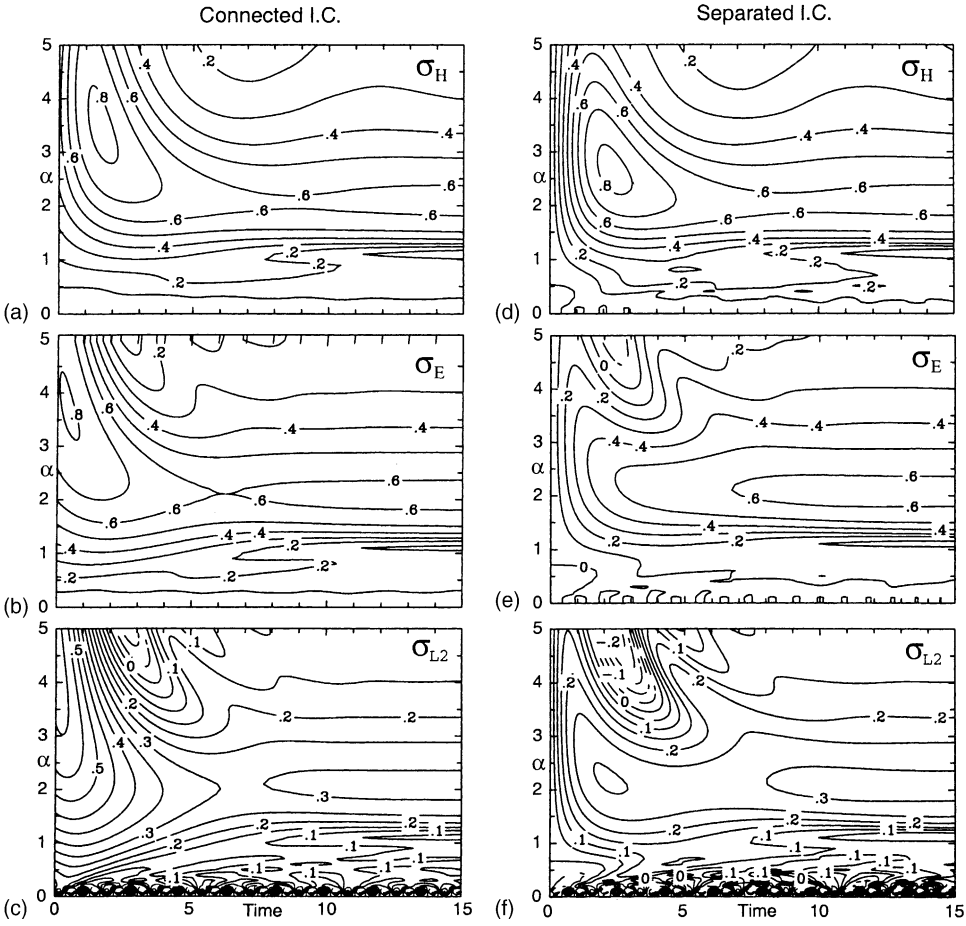

Fig. 2. (a–f) Growth rate time series for the connected (left column) and separated (right column) initial conditions in the G model. The ordinate is absolute wavenumber (α) and the abscissa is nondimensional time in each chart. The top row shows potential enstrophy growth rate, σ_H. The middle row shows total energy growth rate, σ_E. The bottom row displays amplitude growth rate, σ_{L2}. Locations of peak values and corresponding asymptotic normal mode growth rates are reproduced in Table 1. Contour interval of 0.1 for the top two rows and 0.05 for σ_{L2}. NG is largest for eigenmodes much smaller than the most unstable normal mode.

et al. (1982). The Eady model growth rates are broadly similar to the G model results shown in Fig. 2 except that after the initial period of strong NG, the growth rates vacillate between positive and negative values for $\alpha > 2.4$. The other main difference between solutions from the Eady and G models is as follows. While the *H*, *E*, and *L*2 growth rate curves have the same general shape in both models, the peak growth rate and its absolute wavenumber are larger in the Eady model results.

Calculations with the G model using the separated IC differ from those for the connected IC in the following ways.

Table 1
Comparison of peak growth rates found in various growth measures in two versions of the model and for two initial conditions shown in Fig. 1

	Eady model		G model	
	Connected	Separated	Connected	Separated
Max σ_H	0.90	1.26	0.82	0.83
Time	0.99	0.8	1.48	2.40
α	4.5	3.3	3.5	2.5
σ_A	0.0	0.0	0.38	0.57
Max σ_E	0.77	0.56	0.81	0.62
Time	0.05	2.64	0.42	10.6
α	4.6	2.3	3.7	2.1
σ_A	0.0	0.22	0.35	0.62
Max σ_{L2}	0.56	0.31	0.62	0.31
Time	0.02	2.11	0.65	10.9
α	4.7	2.5	4.2	2.1
σ_A	0.0	0.0	0.14	0.31

Data for "square wave" (equal meridional and zonal wavenumbers) solutions are shown. Other data include the time of occurrence of the peak growth rate ("time"), the absolute wavenumber (α), and the asymptotic growth rate (σ_A) for that absolute wavenumber.

- The separated IC has lower peak growth rate in E and $L2$ than the connected IC at all wavenumbers; from this result one concludes that NG in E and $L2$ is also less at all wavenumbers, not just at the most unstable wavelength.
- The wavenumber having the peak NG is different for each growth measure but in general occurs at shorter waves for the connected IC.
- There is much less NG in the $L2$ and E growth measures for the separated IC. However, sizable NG remains in the potential enstrophy. This issue is noted and examined by Hodyss and Grotjahn (2001) for plane waves at the most unstable wavenumber.

Again, broadly similar results are found for the Eady model even for waves shorter than the short wave cut-off. These and other differences are apparent in Table 1.

The ratio of actual growth rate to normal mode growth rate (Γ) has peak values that are much larger and occur at much higher wavenumber for the connected than for the separated case. Peak Γ at $\alpha = 5.0$ is >3.5 for H, E, and $L2$ growth measures in the connected cases. For the separated cases H has peak $\Gamma \sim 2.5$ at $\alpha = 5.0$, while for $L2$ peak $\Gamma = 1.5$ at $\alpha = 4$ and $\Gamma < 1$ for E at all values of α.

Additional understanding of the H growth rates is gained from looking at the components of H. The components of H undergo noteworthy differences in their *individual* rates of growth. For both ICs, BPV is initially quite small and undergoes a rapid growth and structural change to adjust to the profile of the normal mode. The large growth of BPV seen in Fig. 3a and d occurs very early in each simulation. This reflects the rather arbitrary definition of IC using analytic functions. As discussed in Hodyss and Grotjahn (2001) relatively small adjustments in the initial stream function distribution (that cause BPV to differ less from a normal mode BPV profile) cause significant lowering of the peak growth rate. The Eady

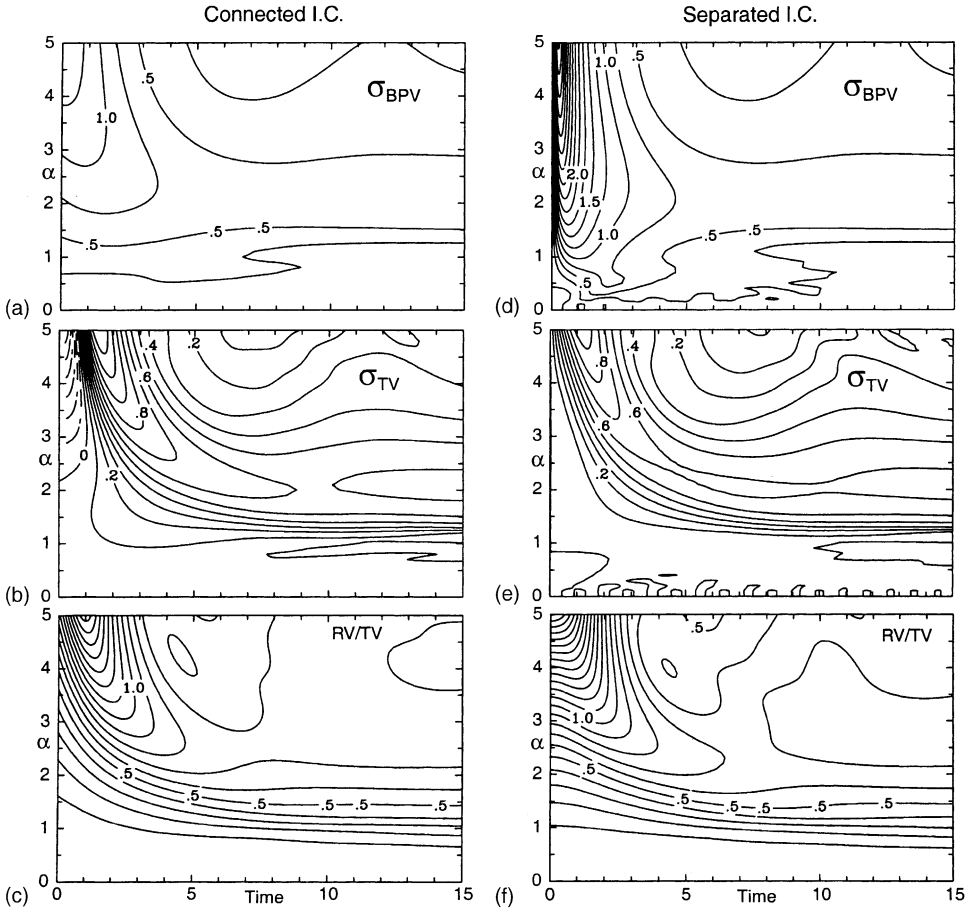

Fig. 3. (a–f) Similar to Fig. 2 except for components of potential enstrophy in G model simulations. Growth rates for BPV squared (top row) using a 0.25 contour interval. Growth rate of TV squared (middle row) uses a 0.1 contour interval as for potential enstrophy (Fig. 2a and d). The growth rate for RV squared is simply twice the values shown for *L*2 (Fig. 2c and f). The ratio of domain average RV over domain average TV is shown (bottom row) with a 0.1 contour interval. σ_{BPV} and σ_{TV} have large NG for very short waves but RV moderates the NG seen in σ_H.

model BPV growth is due to growth along the top and bottom boundaries, but in the G model only the lower boundary is relevant (due to mass weighting). The maximum growth in BPV in Fig. 3d occurs at the same wavenumber and has nearly exactly the same magnitude as that in the Eady model and the overall pattern for all wavenumbers is nearly the same in the Eady model at early times. Of particular note are very large growth rates at very early times. In contrast, the thermal vorticity has small or negative growth rates initially and needs some time to reach peak values (Fig. 3b and e). For the connected IC, TV is initially decaying (for $\alpha > 2.2$) as might be expected for a solution that is mainly tilting into a more vertical orientation early on in the integration. (TV is proportional to the vertical derivatives

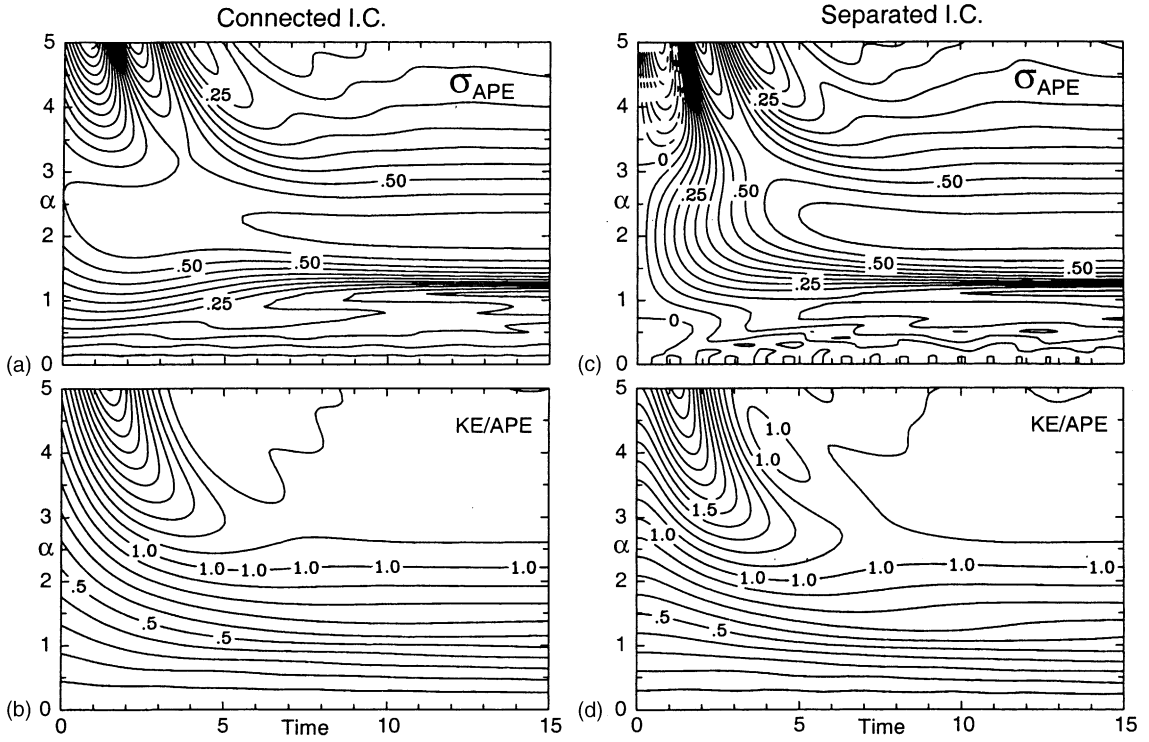

Fig. 4. (a–d) Similar to Fig. 3 except for components of energy in G model simulations. Growth rates for APE (top row) using a 0.05 contour interval. The ratio of domain average KE over domain average APE (bottom row) with contour interval 0.1. The growth rate for KE is simply twice the values shown for $L2$ (Fig. 2c and f). σ_{APE} has large NG for very short waves but KE moderates the NG seen in σ_E.

of stream function and those in turn are proportional to the amount of vertical tilt for the connected case). This initially negative growth increases with decreasing scale. Maximum NG (in Fig. 3b and e) is considerably less than that found in the Eady model (not shown). However, the Eady model solution does have the same general pattern for both ICs. The combination of BPV and TV growth rates is broadly consistent with a peak H growth rate that occurs earlier than the peak for TV but later than that for BPV. Finally, the BPV and TV peak growth rates occur at higher wavenumbers than the range of wavenumbers plotted. But, peak H growth occurs well within the range of wavenumbers plotted. The H growth rate spectrum does so because the fraction due to RV (early on) dramatically increases with wavenumber (Fig. 3c and f). The growth rates of RV are exactly twice the values of $L2$ shown in Fig. 2c and f for this model formulation. Thus for large α, H is mainly RV, RV growth rates decrease with higher wavenumbers, and so do growth rates of H.

The spectrum of total energy growth rates can be understood better by examining growth rates of KE and APE components of E. Growth rates of APE are shown in Fig. 4a and c; sizable oscillations of APE growth occur for short waves. Similar to TV, the largest growth rates occur after a period of small or negative growth rates for the short waves. Also, the peak APE growth rates occur for shorter scales than those plotted. At the largest wavenumber shown ($\alpha = 5.0$) the peak value of Γ is 4.0 for the connected IC and 3.25 for the separated IC. In contrast, for middle wavenumbers ($1 < \alpha < 3.5$) little NG is evident in separated ICs. There is more NG in the connected case APE for wavenumbers $1 < \alpha < 3.5$ but Γ remains close to 1.0 throughout the time integration. Growth rates of KE have the same distribution (but twice the amplitude) as those of $L2$ (Fig. 2) and so are not shown. Instead, the ratio of KE over APE is shown in Fig. 4b and d. The asymptotic spectrum of this ratio is nearly constant at small wavenumbers and approaches zero as the wavenumber approaches zero. However, early in the integration it is clear that KE is a larger fraction of E than is APE for short waves. Consequently, the pattern for E is strongly influenced by the growth of KE for short waves at early times. Since KE and $L2$ have the same growth rate pattern, the $L2$ and E growth measures (Fig. 2) have similar growth rate time series for short wavelengths.

4. Meridionally free solutions

4.1. Introductory comments

In the previous section, meridional structure is specified by a single wavelength Cosine function in the meridional (y) direction. In this section, the initial disturbance has a Gaussian variation in the y-direction. The Gaussian structure function is expressed spectrally using 32 Fourier modes in the y-direction. The zonal direction remains a single wavenumber. The length scale in the y-direction is defined by setting one e-folding length to $L/5$, where L is the zonal wavelength. The resultant IC looks like a chain of highs and lows in the zonal direction only, with each high and low looking approximately like a square wave. The solutions are obtained numerically in a very large channel whose width is scaled to be at least four times the meridional scale as defined above. The disturbance is initially centered in the channel. The (initial) absolute wavenumbers examined vary from 0.1 to 5. Solutions for the Eady and G models use the same basic-state as before; U has vertical shear and no horizontal shear.

4.2. Time series of growth rates

Direct comparison with square waves could be attempted by plotting growth rate spectra using the initial absolute wavenumber (approximately the square root of two times the zonal wavenumber) for the ordinate. Since meridional scale is now allowed to change over time, the comparison will break down after a period of time. Such plots are not shown because they look very similar to Figs. 2–4. (Similar figures, using zonal wavelength, can be found in Hodyss, 1999). Nonetheless, a few noteworthy differences from the square wave solutions occur as follows.

- Peak growth rates (and presumably the strongest NG) occur at even smaller scales.
- Peak growth rates (and hence NG) are larger (in some cases by >35%) for the Gaussian IC.
- The asymptotic growth rates are larger now (especially for zonally short waves) because meridional scale increases over time (for middle and short waves) the dominant absolute wavenumber decreases, which for short waves means larger growth rate.

4.3. Emergence of horizontal tilts

Allowing the meridional structure to evolve leads to interesting changes in the horizontal structure that are not present in the square wave results. So, horizontal structure evolution will be emphasized in this section. The two main differences created by allowing meridional structure to evolve are: (1) the horizontal scale changes over time and; (2) zonal mean eddy momentum fluxes develop. The former is easily explained by the emergence of the more unstable modes. The latter depends upon the phase shifts and phase speeds of the primary constituents at any one time.

Before discussing the specific solutions it is useful to consider how horizontal tilts may occur even though there is no horizontal shear in the basic flow. None of the eigenmodes present has any horizontal tilt. The horizontal tilts occur in the total solution when there is overlapping of eigenmodes having different meridional wavenumber and different zonal phase. Simple examples are illustrated in Fig. 5. Both archetype ICs are composed of many eigenmodes including continuum modes having sizable amplitude. But, the asymptotic structure is dominated solely by the most unstable normal mode. At intermediate times, the solution is typically dominated by just a few of the more unstable normal modes. This "intermediate" time period can be quite lengthy given the initial projections of the unstable modes and a growth rate spectrum whose most unstable modes can have similar growth rates. The actual structure during the intermediate time can vary greatly depending upon the eigenmodes present and their phase relationships. However, one may isolate a few general factors that influence the structure seen:

1. The initial relative phase and projection of the eigenmodes that are more unstable.
2. The amount of upstream tilt with height for each eigenmode (upstream tilt decreases with decreasing growth rate).
3. The phase speed spectrum governing how the eigenmodes separate from an initial phase relation (It is a function of meridional wavenumber, l for given k in the G model). In contrast, the Eady model has the same phase speed for all unstable normal modes.

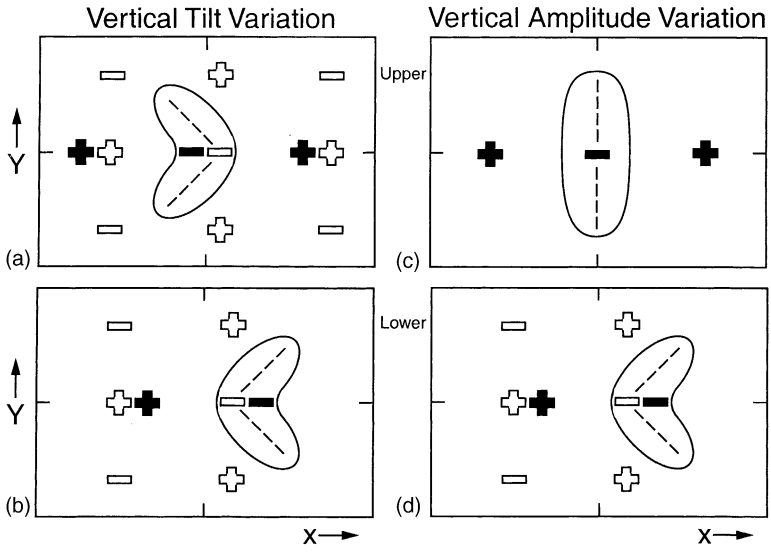

Fig. 5. Schematic diagrams illustrating how two unstable eigenmodes, each without horizontal axis tilts, produce horizontal tilts when combined. Eigenmode maxima and minima are indicated with + and − symbols, respectively. The more unstable mode is depicted with solid +/− symbols while "hollow" symbols are used for the less unstable mode. Relative phases between eigenmodes as well as the upstream tilt can be deduced from the +/− symbols. A solid contour indicates the resultant sum, with dashed lines indicating horizontal trough axes. "Back" tilted troughs appear in (a) and "forward" tilts in (b). Two situations are depicted. (a) and (b) illustrates how horizontal tilts vary with height since less unstable eigenmodes have less upstream tilt. This situation is more likely for middle zonal wavelengths. The "back" tilted trough (a) has non-zero zonal mean eddy momentum convergence; the "forward" tilted trough (b) has eddy momentum divergence. The situation depicted in (c) and (d) is more typical of short zonal wavelengths where less unstable modes are strongly bottom-trapped. So, the upper-level (c) has no significant contribution from the less unstable mode and often develops a larger meridional scale more quickly than the lower level (d) portion of the perturbation. Other combinations are possible as discussed in the text.

4. The vertical structure of the eigenmodes' amplitude (e.g. in Fig. 5d shorter waves are more bottom-trapped and so have less impact at upper-levels).

Item 1 selects the main eigenmodes to interact at an intermediate time. Since the IC is symmetric about $y = 0$, asymmetric unstable modes are excluded. Items 2 and 3 can lead to the development of horizontal tilt. Items 2 and 4 lead to structures that look different at upper and lower levels.

The growth rate spectrum varies such that the most unstable waves have an absolute wavenumber near 2. Consequently, for longer waves ($k < 1$ or zonal wavelength >6000 km in our scaling) the most unstable wave has $l > k$. For shorter waves ($k > 2$, say) the meridional structure is much larger than the zonal structure for the most unstable modes. Hence shorter zonal wavelengths asymptotically develop large meridional scale over time. For a specified k (>1.5), waves with smaller meridional scale (i.e. larger absolute wavenumber) have smaller growth rate, are more bottom-trapped, and have less upstream tilt. Therefore, for zonally short waves, the meridional scale increases more rapidly at upper-levels than at

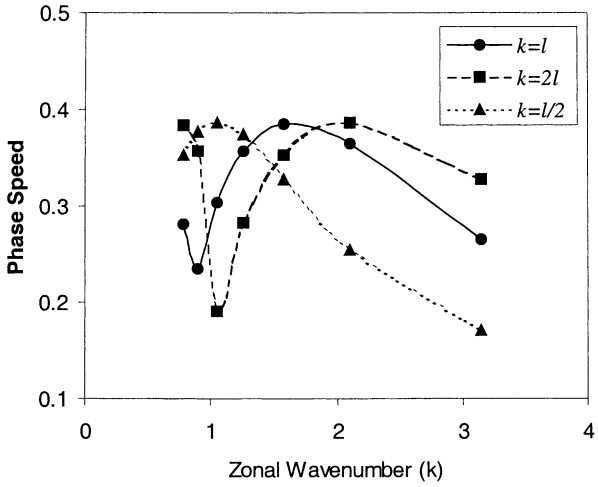

Fig. 6. Phase speeds of some selected growing normal modes in the G model. The scaling assumed has $k = 1.0$ for 6000 km, $k = 1.6$ for 4000 km, and $k = 3.1$ for 2000 km zonal wavelength. Phase speeds of relevant unstable modes tend to decrease with increasing meridional wavenumber for short zonal waves and increase for long zonal waves.

lower levels because only waves with large meridional scale have significant upper-level amplitude.

Observations show increasing meridional and zonal scale of surface lows (Grotjahn et al., 1999) as they develop; but upper-level troughs (Grotjahn and Castello, 2000) do not change scale since they start out large. Also relevant may be Hartmann et al. (1995) who find synoptic scale waves can rapidly develop from much smaller scale singular vectors.

The phase speed spectrum of the *more unstable* waves varies differently for short than for long zonal wavelengths. Fig. 6 illustrates how phase speed varies for a few selected meridional structures. For zonally short waves ($k > 2.5$) small meridional scale eigenmodes tend to move slower than longer meridional scale eigenmodes. If all else is equal, eigenmodes that are in phase will start to separate and their sum develops horizontal tilts similar to Fig. 5b. For longer waves ($k < 1.3$) eigenmodes with small meridional scale tend to move faster than eigenmodes with longer meridional scale. Eigenmodes initially in phase separate to form a sum similar to Fig. 5a. For intermediate waves ($k \sim 2$) the phase speed is similar for eigenmodes of different meridional scale.

The normal mode amplitude for "middle" wavenumbers ($k \sim 2$) has maxima near the surface and near the simulated tropopause. As mentioned, unstable shorter waves emphasize the surface maximum more and more as absolute wavenumber increases. Unstable long waves emphasize the upper maximum.

Fig. 7 shows a time progression of the perturbation pressure field at two levels using the separated IC. The two general changes in eddy structure are seen in this sequence. First, the solution evolves towards a much larger meridional wavelength (commensurate with the most unstable mode present). Second, the "square" wave type of IC quickly develops "bean-like" shapes; these horizontal axis tilts imply eddy momentum fluxes that have non-zero zonal

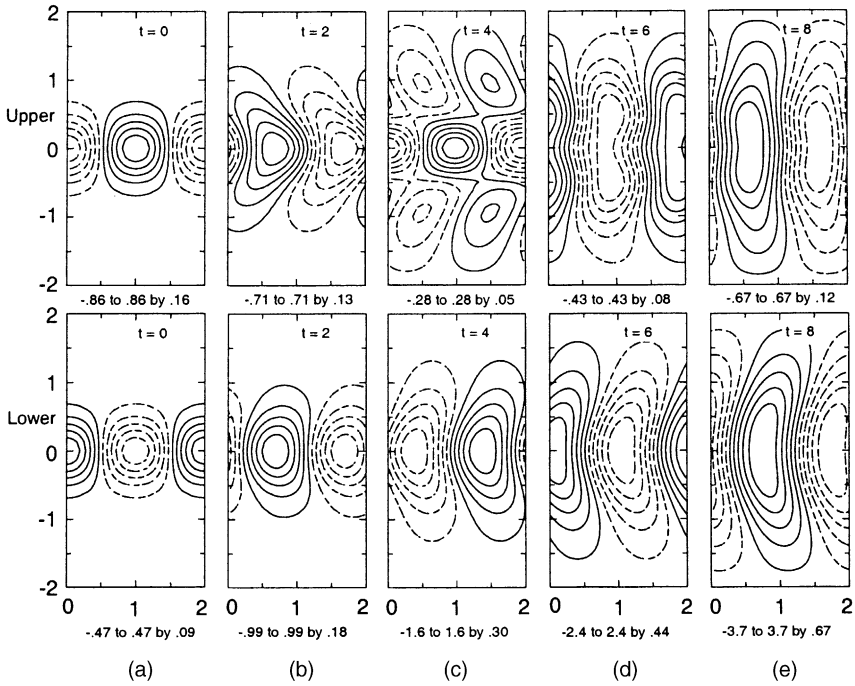

Fig. 7. (a–e) Example time sequence of upper ($z = 1$) and lower ($z = 0$) level eddy pressure fields illustrating the development of horizontal tilts and increasing meridional scale. Results are shown for a short wave ($k = 3.1$) in the G model using Gaussian meridional structure and separated trough initial condition. As the time $t = 2$ results show, the tilts can reverse direction with height. The tilts evolve as the most unstable normal mode emerges. The contour interval varies between the plots and was chosen to make a similar number of contours each time and thereby make the horizontal axis tilts more visible.

means. The nature of the tilts shown at time $t = 2$ happen to have zonal mean momentum convergence at upper-levels and momentum divergence at lower levels. However, the type and amount of tilt varies with the wavenumber, IC, and model used. For example, the total solution for a x wavelength of 7000 km in the G model has very similar appearance at time $t = 2$ to that shown in Fig. 7b (a 2000 km wavelength solution). The sequence also shows that the tilts can vary during the course of the integration. Accordingly, it is difficult to generalize about the nature of the horizontal tilts; however, *in the cases investigated here* eddy momentum convergence structures appeared much more often. This result suggests that phase speed decreasing with meridional wavelength (for fixed k) could be a dominant factor. For middle wavenumbers ($k \sim 2$) the separated IC tends to develop and maintain momentum converging tilts at upper and lower levels; also, the meridional scale increases more rapidly at upper-levels (e.g. Fig. 8b). The connected trough IC for middle waves leads to similar horizontal tilts, though the upper-level increase in scale develops more slowly.

In studies of "realistic" jet flows it seems most common for the eddies to develop "tilted back" structures. This is seen in eigenvalue studies (e.g. Frederiksen, 1979; Grotjahn, 1979) and in initial-value studies (e.g. Simmons and Hoskins, 1979; Grotjahn and Castello, 2002).

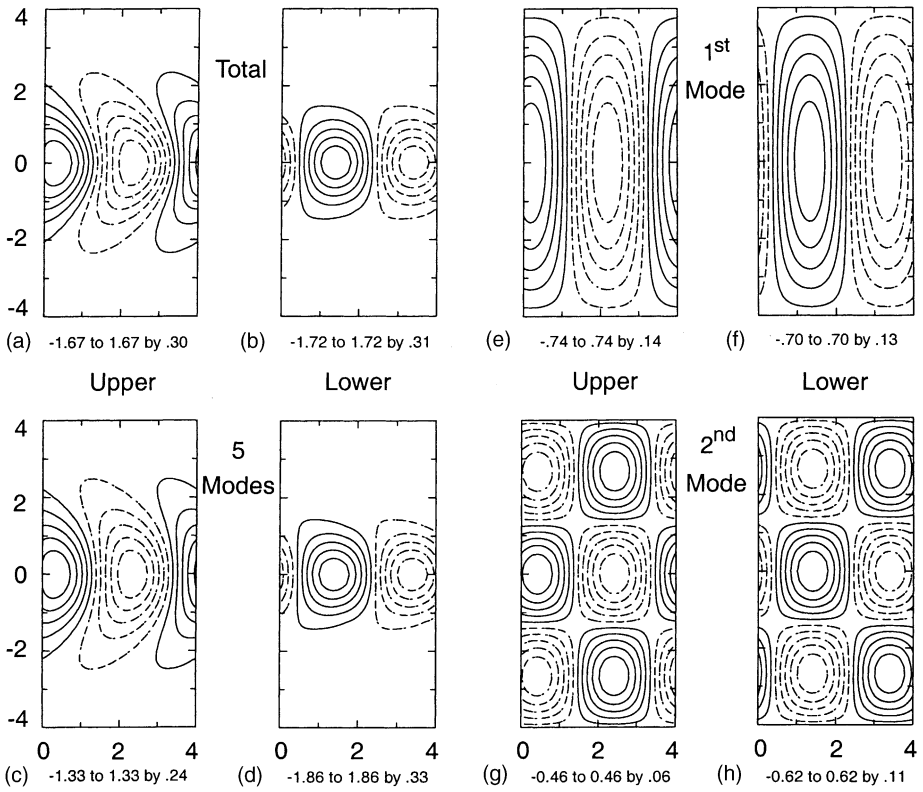

Fig. 8. Depiction of how the tilted structure is reconstructed from a small number of unstable eigenmodes. Results are shown for the G model for a middle zonal wavelength ($k = 1.6$) using the separated initial condition. (a) and (b) are the total solution at time $t = 4$ at upper and lower troposphere, respectively. (c) and (d) are a reconstruction of (a) and (b) using the five unstable normal modes present having the largest projection amplitudes. The mode with largest projection (the most unstable) is shown in (e) and (f) at upper and lower levels. The mode with second largest projection (g) and (h) is also shown. The less unstable mode has less upstream tilt and less upper-level amplitude than the most unstable mode. So, the horizontal tilt and upper scale are larger at upper-levels (c).

As stated above, the tilt that develops varies with the case studied. So, it is unclear how important the overlapping of eigenmodes here is compared to horizontal shear in creating horizontal tilts. Our results can only suggest that an IC that differs from a single normal mode will likely develop horizontal tilts. It may be that "tilted back" horizontal axes are favored by both mechanisms, but further work is needed to establish that conclusion for mean-flow jets.

Interpretation of the horizontal tilts seen (e.g. Fig. 7) is facilitated by decomposing the total solution into a few key eigenmodes at an intermediate time. The total solution at that time can be approximately reconstructed from just a few unstable normal modes. The horizontal tilt seen in the reconstruction and in the total solution can be deduced when these few modes are separately plotted with proper relative phase. The relative phase between these normal modes is thereby easily seen to create the "bean-like" pattern of the total

solution. The smaller upstream tilt for less unstable modes is also apparent. The amplitude and phase of each eigenmode are found by projecting each mode onto the total solution. For the middle wave (4000 km x range; $k = 1.6$) the modal composite is constructed from five of the nine most unstable normal modes. Fig. 8 illustrates such a diagnosis of the total solution at time $t = 4$ for $k = 1.6$. Fig. 8 includes plots of the two normal modes having the largest projection amplitudes.

The Eady model solution for the connected trough IC (and middle wavelengths) develops and maintains tilts similar to Fig. 7b for times after $t = 2$. The horizontal tilts are maintained at both levels, but the meridional scale increases. The persistence of these tilts occurs because this IC has 13% smaller projection onto the most unstable mode than the projection onto the next most unstable mode present. The respective nondimensional growth rates are 0.30 and 0.21 and the phase speeds are identical. Consequently, the eigenmodes maintain the same relative phase and it takes >10 units of time for the most unstable solution to dominate. The more unstable mode (having larger meridional structure) has larger upstream tilt than the next most unstable mode. The two unstable modes match phase at the middle elevation ($z = 0.5$). Below $z = 0.5$ the more unstable mode is ahead and *vice versa* above. The horizontal tilts described here occur even sooner in the Eady model when using the separated IC.

4.4. An application to upper-level PV anomalies

In this section we analyze the scale-dependent behavior of upper-level PV anomalies as an extension to Hakim (2000b). Hakim (2000b) deduced a variety of important results about the upper-level initiation of cyclogenesis by PV anomalies, but he had very little discussion of the scale-dependent behavior of the PV anomalies or the time series of their growth rates as a function of wavenumber. We intend here to fill this gap while also using the more realistic G model.

We will model upper-level precursor disturbances riding along the tropopause as a QGPV anomaly with the following functional form:

$$q = \sin(kx)\left[1 - \left(\frac{y}{\mu_y}\right)^2\right] \exp\left\{-\left[\left(\frac{y}{\mu_y}\right)^2 + \left(\frac{z-1}{\mu_z}\right)^2\right]\right\} \tag{10}$$

where $\mu_z = 0.35$ and μ_y is chosen as $L/5$, where L is the zonal wavelength. These definitions are consistent with the meridionally unconfined section and Hakim (2000b). Recall that the horizontal scale defined here is only the *initial* horizontal scale (α_i = initial total horizontal wavenumber); the dominant horizontal scale can change as the model integrates forward in time and typically increases. The scale change and horizontal tilts discussed above occur here too and will not be discussed further. Note that horizontal scale is defined now as the scale of the QGPV anomaly and not that of the anomaly in the pressure field.

The inversion of (10) into the pressure field results in different structures for different horizontal scales. Because large horizontal scales weight relative vorticity less than thermal vorticity the inversion of (10) results in a pressure field with little vertical structure for large horizontal scales. This can be seen in Fig. 9a. Note that Hakim (2000b) did not include a stratosphere and therefore only included the portion of the IC up to $z = 1$. In Fig. 9a

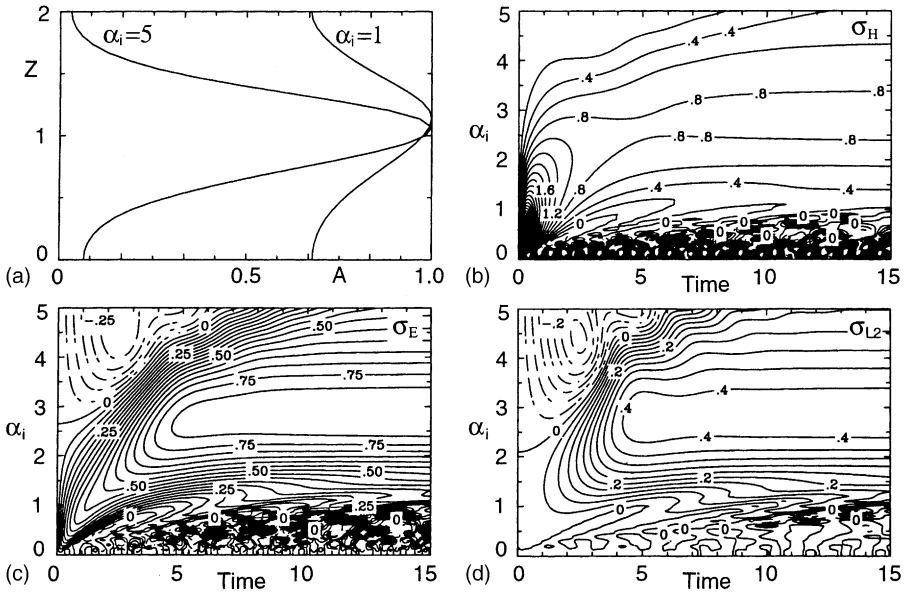

Fig. 9. G model results for an upper-level QGPV anomaly riding along the tropopause. In (a) is shown the initial vertical structure of the QGPV anomaly inverted into the pressure field for two initial horizontal wavenumbers. The ordinate is vertical height z and the abscissa is normalized amplitude. In (b), (c), and (d) is plotted the time series of the growth rate for H, E, and $L2$, respectively. The ordinate is *initial* absolute wavenumber (σ_i) and the abscissa is nondimensional time in each chart. In (b) σ_H is plotted from -12.8 to 36.4 by 0.2, in (c) σ_E is plotted from -0.3 to 0.8 by 0.05, and in (d) σ_{L2} is plotted from -0.28 to 0.4 by 0.04.

is plotted the amplitude variation in the pressure field for (10) at two different horizontal scales. For $\alpha_i = 1$ the vertical structure of the IC in the pressure field is much less vertically localized than for $\alpha_i = 5$. The vertical structure for $\alpha_i < 1$ has almost no noticeable variation with height. We conclude then that small-scale upper-level QGPV anomalies produce localized upper-level pressure anomalies but large-scale upper-level QGPV anomalies produce uniform vertical troughs. This property of (10) will have a profound effect on the time series of the various growth measures.

In Fig. 9b is seen the time series of the growth rate for H. The maximum growth rate in H is extremely large ($\sigma_H = 36$) and occurs at the largest horizontal scales. As discussed above, this is because the largest horizontal scales are associated with a uniform vertical trough that has very little initial BPV. As discussed in Hodyss and Grotjahn (2001) the growth rate of H is highly sensitive to the growth in BPV and the growth of BPV is very large for ICs with little amplitude variation with height. However, for horizontal scales more associated with typical cyclogenesis ($\alpha_i \sim 2$) there is little apparent NG in H. Also, in distinction to our previous results with the connected and separated ICs there is very little NG for the shortest horizontal scales.

In Fig. 9c is seen the time series of the growth rate for E. This growth measure has maximum NG at large horizontal scales too. This is due to the growth in APE dominating that of KE because KE is small for large horizontal scales. However, like the time series

for H there is very little NG at horizontal scales typically associated with cyclogenesis. For $\alpha_i > 3$ there is actually large initial decay in E before growth in this measure begins.

In Fig. 9d is seen the time series of the growth rate for $L2$. The growth rate time series for $L2$ shows the least NG of any of the growth measures shown in Fig. 9. At all horizontal scales shown in Fig. 9 the growth in $L2$ shows very little growth until about $t = 5$. This growth around $t = 5$ appears to be associated with the emergence of the most unstable normal mode. The large NG at large horizontal scale is very much reduced. There is large negative growth in $L2$ at short horizontal scales, which suggests that the large negative growth in E at short horizontal scales is likely due to large negative growth in KE.

5. Conclusions

This report considers how the relative importance of nonmodal growth (NG) and unstable normal mode growth varies with the scale and structure of the cyclone. Since an observed cyclone usually has the same length scale in the meridional and zonal directions, initial conditions (ICs) used here also have similar length scales in these two directions. In simulations labeled "square waves" the zonal wavenumber (k) and meridional wavenumber (l) are equal throughout the integration. In "meridionally free" integrations, the meridional structure is free to evolve. The initial vertical structure is defined by one of two ICs.

Each IC is an archetype for a broader class of ICs. One IC has troughs and ridges of uniform amplitude tilted upstream with height in the troposphere. The other IC has separate troughs and ridges in lower and upper troposphere and all are without upstream tilt. The former IC is labeled "connected" and has been shown to have large NG in prior studies. The latter IC, labeled "separated", is more similar to observed troughs prior to cyclogenesis. The "G" model is a linear, quasi-geostrophic model that allows compressibility, realistic static stability, and linear Coriolis parameter variation. Further approximations may be introduced to obtain "Eady" model simulations.

The NG mechanism becomes more prominent for short waves. This result is seen in all the growth rates tracked: potential enstrophy, energy, and their components, as well as amplitude. The peak growth rates occur for short zonal wavelengths. Since the normal mode growth rates are small at these scales, these peak values (and hence NG) exceed the asymptotic value by a much larger percentage than for middle wavelengths. (The asymptotic value is dictated by the most unstable normal mode present.) These results are seen for both ICs and in both Eady and G model formulations. Similar results are found when the meridional structure is free to evolve from a Gaussian IC having a meridional scale chosen to correspond to the zonal scale. The peak growth rates of boundary potential vorticity (BPV), "thermal" vorticity (TV), and available potential energy (APE) all tend to occur at very large zonal wavenumber. Peak growth rates of total energy (E) and potential enstrophy (H) occur at much longer scales in part due to the moderating influence of the amplitude growth rates. The amplitude norm ($L2$) has peak growth rate at a middle wavelength for the separated IC. For the connected IC, $L2$ and KE have large initial growth for small waves but that is opposed by the APE which has initially negative growth rate as upstream tilt decreases early on. Amplitude growth is relevant since the pattern is equivalent (with values twice as large) for relative vorticity (RV) and KE. Early on, RV and KE are large fractions of H

and *E*, respectively, for these shortest waves. The primary difference for the ICs is that the peak growth rates are systematically less for the separated IC at *all* wavenumbers. Grotjahn and Tribbia (1995) found the separated IC to have less NG when they considered only the most unstable wavelength (and a single meridional scale). Here, we find this result to be generally valid for the wavenumbers tested, even when meridional structure is allowed to freely evolve.

When the solutions are allowed to freely evolve in the meridional direction the meridional scale changes and horizontal tilts develop even though there is no horizontal shear in the mean-flow. The scale changes commensurate with the emergence of the most unstable mode. For middle and short zonal wavenumbers, the meridional scale of the most unstable mode is much larger than the zonal scale. Presumably, introduction of meridional shear (forming an internal jet) could remove much of this meridional scale change. If the basic-state has meridional shear, such shear introduces a meridional length scale into the problem. That meridional shear would cause the most unstable normal modes to prefer a similar meridional length scale and thereby oppose some of the meridional scale increase found here. Eigenmodes for basic flows having across-flow shear have horizontal tilts. However, the mechanism that generates the tilts seen here still applies. It is beyond the scope of this study to examine how the two sources of horizontal tilt would compare.

Despite the lack of basic-state horizontal shear, eddies develop horizontal tilts when the solutions are allowed to evolve freely in the meridional direction. Such tilts imply non-zero zonal mean eddy momentum convergence ("tilted back") or divergence ("tilted forward") depending upon the orientation (e.g. Figs. 4 and 9, Grotjahn, 1993). While "tilted back" patterns are more common in these integration's, examples of forward tilts occur. It is not difficult to find instances of opposite tilts at upper and lower levels. These solutions are diagnosed by projecting the total solution onto the linear eigenmodes. At intermediate times, much of the total solution is captured by a few of the most unstable eigenmodes having the largest projections. Such analysis makes clear that the overlapping of these eigenmodes having different relative phases leads to the horizontal tilts. The structure that develops depends upon three things: how phase speed varies with the meridional scale of each mode present, the amount of upstream tilt with height each mode has, and the amplitude variation with height of each mode. In general, the shorter waves tend to develop "forward" tilts at lower levels (creating zonal mean eddy momentum divergence). Short wave forward tilts are consistent with the phase speed spectrum, which decreases for less unstable and more bottom-trapped eigenmodes. The situation is different for intermediate waves. Intermediate waves have horizontal tilts that sometimes reverse between upper and lower troposphere. In our results, intermediate waves develop "back" tilts most frequently (especially at upper-levels).

The horizontal tilts are transitory, but "back" tilts of intermediate waves could be self-reinforcing. Such tilts create zonal mean eddy momentum convergence that forms a weak jet along the meridional center axis of the eddies. Even early studies (e.g. Grotjahn, 1979 in Cartesian geometry; Simmons and Hoskins, 1977 in Spherical geometry) find that eigenmodes for an internal jet have "back" tilts.

Cyclogenesis is typically associated with upper-level PV structures riding along the tropopause. We simulate this type of precursor disturbance with an isolated upper-level QGPV IC similar to Hakim (2000b). This IC, when inverted into the pressure field, results

in a vertically isolated pressure anomaly for short horizontal scales and a nearly uniform vertical trough for large horizontal scales. This illustrates an important property that one must be aware of when examining ICs in initial-value simulations. Fixing the structure of a specific QGPV anomaly and varying its horizontal scale results in differing vertical structures in the pressure field at each of those horizontal scales. The converse is also true and applies directly to the present study; fixing the vertical structure in the pressure field and varying the horizontal scale results in different QGPV structures at different horizontal scales.

At horizontal scales typical of cyclogenesis, upper-level QGPV anomalies in the G model have little NG in *E*, *H*, and *L*2. There is large NG at very long horizontal scales in *H* and *E*. This is due to the vertical structure of the IC at long horizontal scales being that of a uniform vertical trough. As discussed in Hodyss and Grotjahn (2001) ICs with little amplitude variation with height (e.g. uniform vertical troughs) have large *E* and *H* growth rates because these ICs have little BPV, TV, and APE initially but unstable normal modes typically have large values of these parameters. Therefore, the transition through time as the solution changes from a uniform vertical trough into that of the unstable normal mode will generally result in large *E* and *H* growth rates.

Our results for upper-level QGPV anomalies show much less NG than the results of Hakim (2000b). Hakim (2000b) examines an initial QGPV anomaly with a horizontal scale by our definition of approximately $\alpha_{\mathrm{i}} = 2.6$. Our results and Hakim's both show very little NG in the *L*2 norm. However, Hakim finds moderate NG in both *E* and *H* while at $\alpha_{\mathrm{i}} = 2.6$ our results show no NG. This is presumably due to the substantial model differences between our two studies. For example, Hakim uses the Eady model whereas we are using the more realistic basic-state (including a stratosphere) associated with the G model. Another important difference is Hakim's IC is localized in the *x-direc*tion and ours is constrained to be sinusoidal with a single wavenumber in the *x-direc*tion. Because of this lack of constraint Hakim's IC develops a large upper-level ridge out ahead of the initial trough (see his Fig. 1). The development of large growth rates in *E* and *H* could be due in part to the emergence of new features, which are not allowed to develop in our study.

Acknowledgements

This work was performed in partial fulfillment of the first authors MS degree. DH would like to acknowledge the helpful conversations provided through the course of this work with Dr. T. Nathan, Dr. J. Tribbia and Dr. E. O'Brien. Also, the authors would like to acknowledge the generous support provided by the National Science Foundation through grant ATM-96-15316.

References

Badger, J., Hoskins, B.J., 2001. Simple initial-value problems and mechanisms for baroclinic growth. J. Atmos. Sci. 58, 38–49.

Bretherton, F., 1966. Critical layer instability in baroclinic flows. Q. J. R. Meteor. Soc. 92, 325–334.

Davies, H., Bishop, C., 1994. Eady edge waves and rapid development. J. Atmos. Sci. 51, 1930–1946.

Eady, E., 1949. Long waves and cyclone waves. Tellus 1, 33–52.

Farrell, B., 1982. The initial growth of disturbances in a baroclinic flow. J. Atmos. Sci. 39, 1663–1686.
Farrell, B., 1984. Modal and nonmodal baroclinic waves. J. Atmos. Sci. 41, 668–673.
Farrell, B., 1989. Optimal excitation of baroclinic waves. J. Atmos. Sci. 46, 1193–1206.
Frederiksen, J.S., 1979. Baroclinic instability of zonal flows and planetary waves in multi-level models on a sphere. J. Atmos. Sci. 36, 2320–2335.
Green, J., 1960. A problem in baroclinic stability. Q. J. R. Meteor. Soc. 86, 237–251.
Grotjahn, R., 1979. Cyclone development along weak thermal fronts. J. Atmos. Sci. 36, 2049–2974.
Grotjahn, R., 1980. Linearized tropopause dynamics and cyclone development. J. Atmos. Sci. 37, 2396–2406.
Grotjahn, R., 1993. Global Atmospheric Circulations, Observations and Theories. Oxford University Press, New York, 430 pp.
Grotjahn, R., 1996. Composite trough evolution of selected west pacific extratropical cyclones. Mon. Wea. Rev. 124, 1470–1479.
Grotjahn, R., Castello, C., 2000. A study of frontal cyclone surface and 300-h Pa geostrophic kinetic energy distribution and scale change. Mon. Wea. Rev. 128, 2865–2874.
Grotjahn, R., Castello, C., 2002. Nonmodal growth on a sphere at various horizontal scales. Geophys. Astrophys. Fluid Dyn. 96, 223–238.
Grotjahn, R., Hodyss, D., Castello, C., 1999. Do frontal cyclones change size? Observed widths of north pacific lows. Mon. Wea. Rev. 127, 1089–1095.
Grotjahn, R., Pedersen, R., Tribbia, J., 1995. Linear instability with Ekinan and interior friction. Part II: Initial-value analysis. J. Atmos. Sci. 52, 764–777.
Grotjahn, R., Tribbia, J., 1995. On the mechanism of cyclogenesis as deduced from vertical axis tilts. Tellus 47A, 629–637.
Hakim, G., 2000a. Climatology of coherent structures on the extratropical tropopause. Mon. Wea. Rev. 128, 385–406.
Hakim, G., 2000b. Role of nonmodal growth and nonlinearity in cyclogenesis initial-value problems. J. Atmos. Sci. 57, 2951–2967.
Hartmann, D., Buizza, R., Palmer, T., 1995. Singular vectors: the effect of spatial scale on linear growth of disturbances. J. Atmos. Sci. 52, 3885–3894.
Hodyss, D., 1999. On the effects of vertical and meridional structure to the initial growth of a baroclinic wave. MS Thesis, Department of Land, Air, and Water Resources, University of California, Davis, 112 pp.
Hodyss, D., Grotjahn, R., 2001. Diagnosing cyclogenesis by partitioning energy and potential enstrophy in a linear quasi-geostrophic model. Tellus 53A, 567–577.
Lindzen, R., Tung, K., 1978. Wave overreflection and shear instability. J. Atmos. Sci. 35, 1626–1632.
Lindzen, R., Farrell, B., Jacqmin, D., 1982. Vacillations due to wave interference: applications to the atmosphere and to annulus experiments. J. Atmos. Sci. 39, 14–23.
O'Brien, E., 1992. Optimal growth rates in the quasigeostrophic initial-value problem. J. Atmos. Sci. 49, 1557–1571.
Petterssen, S., Smebye, S., 1971. On the development of extratropical cyclones. Q. J. R. Meteor. Soc. 97, 457–482.
Simmons, A., Hoskins, B., 1977. Baroclinic instability on a sphere: solutions with a more realistic tropopause. J. Atmos. Sci. 34, 581–588.
Simmons, A., Hoskins, B., 1979. The downstream and upstream development of unstable baroclinic waves. J. Atmos. Sci. 36, 1239–1254.
Takayabu, I., 1991. Coupling development: an efficient mechanism for the development of extratropical cyclones. J. Meteor. Soc. Jpn. 69, 837–841.